A Novel Baseband Faster-Than-Nyquist Non-Orthogonal FDM IM/DD System With Block Segmented Soft-Decision Decoder

Zhouyi Hu, *Student Member, IEEE*, and Chun-Kit Chan, *Senior Member, IEEE*

***Abstract*—In this paper, we systematically investigate our recently proposed faster-than-Nyquist non-orthogonal frequency-division multiplexing (FTN-NOFDM) generation technique for intensity modulation/direct detection (IM/DD) optical systems. The proposed scheme is based on modified fractional discrete Fourier transform (mFrDFT), and presents several advantages compared to other existing generation methods. Due to the exemption of guard bands, the proposed scheme achieves higher tolerance to narrow-bandwidth filtering. Besides, without the constraints on compression factor and modulation formats, the proposed system gives better signal flexibility and compatibility to various advanced signal processing techniques. To meet the demand on a large number of FTN-NOFDM subcarriers and high-order modulation formats, we further propose an efficient block segmented soft-decision decoder (BSSDD), which does not need to adjust the signal architecture or sacrifice the spectral efficiency. A 22.24-Gb/s 4-QAM FTN-NOFDM signal with up to 25% bandwidth saving has been successfully implemented over 20-km standard single mode fiber (SSMF) in an IM/DD optical communication system while keeping the bit error ratio (BER) below the hard-decision forward error correction (HD-FEC) limit. For both 4-QAM and 16-QAM FTN-NOFDM systems, the proposed BSSDD achieves better performance than the conventional decoder. All the results indicate that the proposed FTN-NOFDM technique has great potential to be used in high-speed IM/DD optical systems.**

***Index Terms*—Faster-than-nyquist no-orthogonal frequency-division multiplexing (FTN-NOFDM), fixed sphere decoder, intensity modulation/direct detection (IM/DD) optical systems, soft decision.**

I. Introduction

OPTICAL transmission systems are mainly classified into two types: coherent systems and direct-detection (DD) systems. Despite the ultimate performance in receiver sensitivity, spectral efficiency (SE), and robustness against chromatic dispersion (CD), the coherent optical systems are of high system cost and complexity in some specific applications [1]. Hence, the intensity modulation/direct detection (IM/DD) optical system is a promising candidate for the cost-sensitive and short-range scenarios, such as passive optical networks (PONs), data center interconnects and visible light communications (VLC) [2]–[4], at the tradeoff of the SE.

In 1975, J. E. Mazo found that the accelerated signal with ideal soft-decision detection can achieve higher data rate, without damage to the error rate, even if the orthogonality has been violated. Different from Nyquist limit in the orthogonal system, the limit of faster-than-Nyquist (FTN) signaling was termed as Mazo limit [5], [6]. Recently, several technologies based on the concept of FTN signaling have been reported to save bandwidth [7]–[11], in either time domain or frequency domain, which is named as time-squeeze and frequency-squeeze, respectively. In [8], the single-carrier FTN signaling was implemented by pulse shaping and error correction coding. In [9], a multi-carrier system, termed as spectrally efficient frequency division multiplexing (SEFDM), or FTN non-orthogonal frequency-division multiplexing (FTN-NOFDM), was proposed. With closer carrier frequency separation than the conventional orthogonal frequency-division multiplexing (OFDM), FTN-NOFDM further improved the SE in both wireless and optical communication systems. However, the inverse fractional Fourier transform (IFrFT) employed in the conventional FTN-NOFDM system would change the frequency distribution of the subcarriers. As a result, Hermitian symmetry could not be used to generate a real-valued signal, which is different from the DC-biased optical OFDM (DCO-OFDM). Hence, the traditional implementation of the FTN-NOFDM in an IM/DD optical system required signal up-conversion, leading to the increased system complexity and the additional guard bands. Fractional Hartley transform (FrHT) [10] and fractional cosine transform (FrCT) [11] based FTN-NOFDM have been reported to tackle this issue, but only pulse amplitude modulation (PAM) format has been supported. This constraint would limit the application of some advanced signal formats, such as set-partitioned quadrature amplitude modulation (SP-QAM) [12] and offset-QAM [13]. As reported in references [14] and [15], we have recently designed a novel modified fractional discrete Fourier transform (mFrDFT) based technique to implement an IM/DD FTN-NOFDM system, which has shown better signal flexibility and compatibility. However, the brief comparison presented in our previous work is far from satisfactory. Hence, in this paper, we fully investigate mFrDFT and compare it with other existing algorithms in

Manuscript received April 24, 2019; revised August 13, 2019; accepted October 3, 2019. Date of publication October 14, 2019; date of current version February 1, 2020. *(Corresponding author: Chun-Kit Chan.)*

The authors are with the Department of Information Engineering, The Chinese University of Hong Kong, Hong Kong (e-mail: hz016@ie.cuhk.edu.hk; ckchan@ie.cuhk.edu.hk).

Color versions of one or more of the figures in this article are available online at http://ieeexplore.ieee.org.

Digital Object Identifier 10.1109/JLT.2019.2947176

different aspects, including complexity, performance, compatibility, and so on, to verify the superior performance of the proposed technique. Besides, in this paper, we further propose a novel soft-decision decoder to improve the performance of a large-size FTN-NOFDM system.

The main challenge of FTN-NOFDM was its self-created inter-carrier interference (ICI). To tackle this issue, several algorithms have been proposed. In [16], a decoder based on iterative detection (ID) was proposed and has been widely used in FTN-NOFDM systems with relatively low computational complexity. Recently, an algorithm [17] modified from ID, termed as cascaded binary-phase-shift-keying iterative detection (CBID), was designed, which showed the improved performance. In [18], a hybrid detector combining ID and fixed sphere decoding (FSD) was proposed and achieved a quasi-optimum performance. However, the computational complexity of such ID-FSD grew exponentially as the number of subcarriers increases, which made this detector only suitable for small size FTN-NOFDM systems. In [19], a multi-band architecture employing block efficient detector (BED) was reported to implement a large signal dimension for FTN-NOFDM signals, but at the expense of reducing the SE.

In this paper, we systematically investigate our recently proposed mFrDFT based FTN-NOFDM technique [14], [15], and discuss the comparison of mFrDFT and other existing generation methods in details. Furthermore, a modified soft-decision decoder, termed as block segmented soft-decision decoder (BSSDD), is proposed to eliminate the inherent ICI of FTN-NOFDM systems. The proposed decoder can be efficiently employed in a large-size FTN-NOFDM system without any adaptation of the signal architecture or sacrifice the SE. In this work, 22.24-Gb/s 4-QAM/16-QAM FTN-NOFDM signals with employing BSSDD have been successfully implemented in an IM/DD optical communication system. We further experimentally demonstrate that, with large-size and high-order modulation, the proposed BSSDD can concurrently optimize the performance and the complexity.

The rest of the paper is organized as follows: Section II briefly presents the existing methods for implementing FTN-NOFDM in an IM/DD optical system. Section III illustrates the principle of the proposed mFrDFT based FTN-NOFDM system and BSSDD. Section IV describes the experiments to verify the feasibility of the proposed scheme. Section V presents the experimental results and the discussions. Section VI summarizes the paper.

II. Existing Implementations of FTN-NOFDM

The basic principle of FTN-NOFDM is illustrated in Fig. 1. We can see from the sketched spectrum that the subcarrier spacing of FTN-NOFDM is compressed to α (<1) of its original spacing in the conventional OFDM. Hence, with such violation of orthogonality, the overall bandwidth can be further saved. Several algorithms have been reported to generate an FTN-NOFDM signal. It should be noted that some of them should be modified to adapt in an IM/DD optical system.

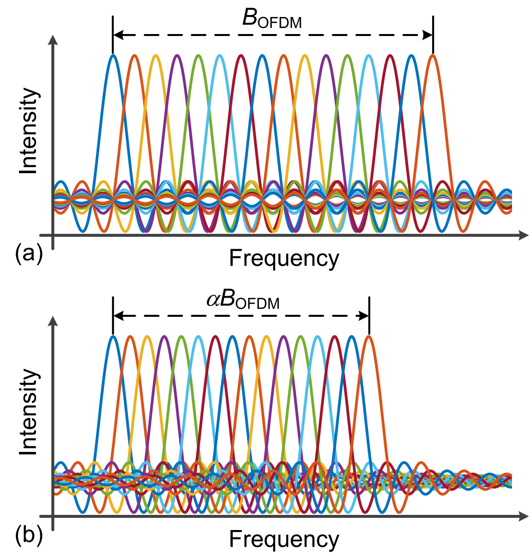

Fig. 1. The sketched spectra of (a) OFDM and (b) FTN-NOFDM ($\alpha = 0.8$).

A. IFrFT Based FTN-NOFDM

In the conventional generation of an FTN-NOFDM signal, IFrFT is utilized [20]. The kth time sample ($k = 0, 1, \ldots, N-1$) of one FTN-NOFDM symbol X can be represented as

$$X[k] = \frac{1}{\sqrt{N}} \sum_{n=0}^{N-1} s_n e^{\frac{j2\pi nk\alpha}{N}}, \quad (1)$$

where $S = [s_0, s_1, \ldots, s_{N-1}]$ denotes the mapped symbols in the frequency domain, N is the number of subcarriers, and α (<1) denotes the compression factor. The orthogonality principle is purposely violated to accommodate faster than the Nyquist rate. However, such IFrFT changes the frequency distribution of subcarriers. In this case, the real-valued signal cannot be generated by employing Hermitian symmetry. Hence, as reported in [20]–[22], the up-conversion is applied to the complex-valued FTN-NOFDM signal for implementing intensity modulation, where both analog and digital methods can be adopted. However, both methods would result in the additional guard bands between the optical carrier and the carried signal, which disserves the tolerance to narrow-bandwidth filtering.

B. IDFT Based FTN-NOFDM

Recently, two hardware-friendly FTN-NOFDM modulation algorithms based on inverse discrete Fourier transform (IDFT) were proposed, either using a single IDFT operation or multiple IDFTs [23], [24].

As shown in Fig. 2, the single IDFT based modulation algorithm can be modified to generate a real-valued FTN-NOFDM signal via Hermitian symmetry. The transmitted QAM symbols are first converted into M ($M < N/2$) parallel channels, and then allocated into M subcarriers of an (N/α)-point IDFT, i.e., from the 1-st subcarrier to the M-th subcarrier, where the DC component (0-th subcarrier) is unfilled. To implement a real-valued signal, the subcarriers from $(N/\alpha) - M$ to $(N/\alpha) - 1$

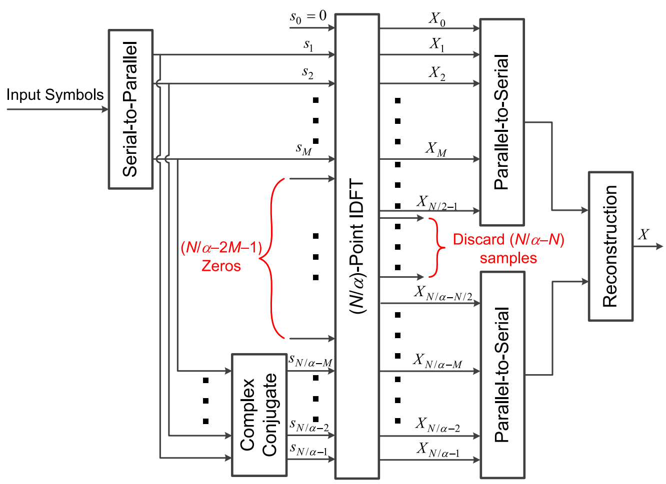

Fig. 2. Block diagram of the real-valued FTN-NOFDM signal generation based on a single IDFT operation.

are modulated by the corresponding symbols with Hermitian symmetry. The remaining subcarriers are set to zero for bandwidth compression. After performing (N/α)-point IDFT, the additional $(N/\alpha - N)$ samples in the time domain are discarded to realize FTN-NOFDM modulation. However, by using such an algorithm, the ratio of N to α has to be an integer value, which limits the flexibility of the system.

To tackle this issue, the multi IDFTs based FTN-NOFDM signal generation method was proposed [23]. In such case, the value of α should be a rational number, i.e., $\alpha = b/c$. Then, the FTN-NOFDM signal with an arbitrary compression factor can be generated using c IDFT operations, where each operation has N points. However, this method would increase the overall complexity. For instance, we have a compression factor of $\alpha = 0.85 = 17/20$. Then, a total of 20 IDFT operations are required for implementation, which is intolerable for some scenarios. Moreover, in this algorithm, Hermitian symmetry cannot be employed directly to obtain a real-valued signal.

C. FrHT/FrCT Based FTN-NOFDM

Since both Hartley transform and cosine transform are real-valued transforms, the FrHT and the FrCT based algorithms were recently proposed for directly generating a real-valued FTN-NOFDM signal in the baseband [10], [11]. At the transmitter side, the signal can be generated by either using inverse FrHT (IFrHT), which is defined as

$$X[k] = \frac{1}{\sqrt{N}} \sum_{n=0}^{N-1} s_n \mathrm{cas}\left(\frac{2\pi n k \alpha}{N}\right), \tag{2}$$

where

$$\mathrm{cas}(\bullet) = \cos(\bullet) + \sin(\bullet) \tag{3}$$

or using inverse FrCT (IFrCT), which is defined as

$$X[k] = \sqrt{\frac{2}{N}} \sum_{n=0}^{N-1} W_n s_n \cos\left(\frac{\pi\alpha(2k+1)n}{2N}\right), \tag{4}$$

where

$$W_n = \begin{cases} \frac{1}{\sqrt{2}}, & n = 0 \\ 1, & n = 1, 2, \cdots, N-1 \end{cases}. \tag{5}$$

However, both algorithms are not suitable for complex-valued modulation formats, leading to the relatively poor compatibility to some advanced digital signal processing (DSP) techniques, such as SP-QAM and offset-QAM. Moreover, due to its inherent properties, only when α is set to 0.5, the FrHT based FTN-NOFDM signal can achieve the same baseband bandwidth as that of the conventional DCO-OFDM, which would result in the additional degradation compared to the IFrFT based method [10].

III. Principle of the Proposed FTN-NOFDM System

In view of the issues discussed above, we recently proposed an mFrDFT based FTN-NOFDM technique [14], [15], which showed the relatively low complexity and improved compatibility in IM/DD optical systems without the additional degradation. To further enhance the system flexibility, a modified soft-decision decoder named BSSDD is presented in this work. The proposed decoder improves the performance of signal detection in a large-size FTN-NOFDM system and is also suitable for high order modulation formats.

A. mFrDFT Based FTN-NOFDM

In the proposed mFrDFT based FTN-NOFDM system, the modulated signal can be expressed by

$$X = FS, \tag{6}$$

where F is an $N \times N$ inverse mFrDFT (ImFrDFT) matrix. The matrix is given in the following:

$$F = \frac{1}{\sqrt{N}} \times \begin{bmatrix} \ddots & & & & \\ & e^{\beta k_1 n_1} & \cdots & e^{\beta k_1 (N/\alpha - N + n_2)} & \\ & \vdots & \ddots & \vdots & \\ & e^{\beta n_1 (N/\alpha - N + k_2)} & \cdots & e^{\beta (N-k_2)(N-n_2)} & \\ & & & & \ddots \end{bmatrix}, \tag{7}$$

where $\beta = j2\pi\alpha/N$. $k_1 = 0, 1, \ldots, N/2 - 1$ and $k_2 = N/2+1, N/2 + 2, \ldots, N - 1$ denote the row indices. $n_1 = 0, 1, \ldots, N/2 - 1$ and $n_2 = N/2 + 1, N/2 + 2, \ldots, N - 1$ denote the column indices. From Eq. (7), it should be noted that F is divided into four submatrices partitioned by the $(N/2)$-th row and the $(N/2)$-th column. To ensure the symmetry of the frequency distribution of the subcarriers, the elements of such row and column are set to the zero-frequency region, i.e., $e^{j\pi n_1}/e^{j\pi n_2}$ and $e^{j\pi k_1}/e^{j\pi k_2}$, respectively. It can be noticed that F is equivalent to the standard IDFT matrix when $\alpha = 1$.

As shown in Fig. 3, after employing Hermitian symmetry, the electrical spectra of different signals are depicted, where N is set

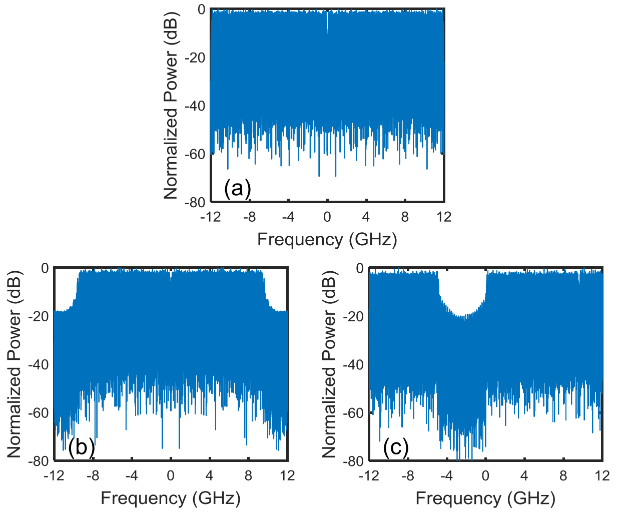

Fig. 3. The electrical spectra of (a) OFDM signal ($N = 128$, $\alpha = 1$), (b) the proposed mFrDFT based FTN-NOFDM signal ($N = 128$, $\alpha = 0.8$), and (c) the conventional IFrFT based FTN-NOFDM signal ($N = 128$, $\alpha = 0.8$) with Hermitian symmetry.

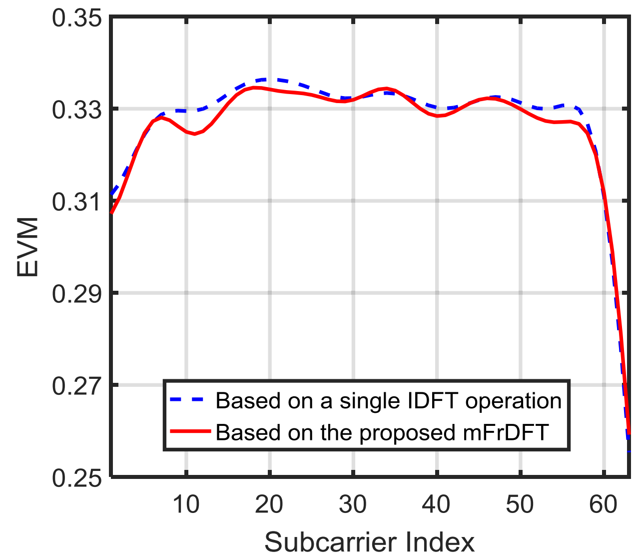

Fig. 4. EVM versus subcarrier index for the method based on a single IDFT operation and the proposed mFrDFT ($\alpha = 8/9$).

to 128. Fig. 3(a) and (b) show the spectrum of a DCO-OFDM signal ($\alpha = 1$) and an FTN-NOFDM signal ($\alpha = 0.8$) using the mFrDFT based method, respectively. We can see from the two figures that the modulated subcarriers are centered around the DC carrier, which can both ensure the real-valued signal in the time domain. However, with the conventional FTN-NOFDM signal generation method described in Eq. (1), the frequency distribution of subcarriers is changed, as shown in Fig. 3(c). Hence, a real-valued FTN-NOFDM signal cannot be obtained by employing Hermitian symmetry in this case.

Compared to the single IDFT based modulation algorithm illustrated in Fig. 2, the proposed method also achieves an improved performance, in addition to its no constraint on the value of α. When $\alpha = 8/9$ and 63/128 subcarriers are effectively modulated by 4-QAM symbols, the estimated error vector magnitude (EVM) versus the index of subcarriers for two different real-valued FTN-NOFDM signals is presented in Fig. 4. We can see from the figure that the proposed scheme achieves a slightly lower EVM curve compared to the single IDFT based method, which can be attributed to its relatively lower power leakage into unmodulated subcarriers. It should be noted that both FTN-NOFDM signals were demodulated without employing any additional soft-decision decoders. Hence, the EVM performance of the two cases would be both improved significantly in the practical system.

The detailed comparison of different methods implementing a real-valued FTN-NOFDM signal is summarized in Table I. It is clear that the proposed mFrDFT based generation method has the highest flexibility and compatibility, indicating its great potential to be used in an FTN-NOFDM IM/DD optical system.

TABLE I
COMPARISON OF DIFFERENT METHODS

Method	Upconversion	Constraint on α	Constraint on formats	Additional degradation
IFrFT [16]	Yes	No	No	No
IDFT [19]	No	Yes	No	No
FrHT [8]	No	No	Yes	Yes
FrCT [9]	No	No	Yes	No
mFrDFT	No	No	No	No

B. Block Segmented Soft-Decision Decoder

At the receiver side of an FTN-NOFDM system, the captured signal is first demodulated by the mFrDFT matrix defined as the conjugate matrix F^*. The initially demodulated signal can be expressed by

$$R = F^* \hat{X}, \tag{8}$$

where $\hat{X}$ is the received signal after transmission over a noisy and fading channel. Due to the self-created ICI from FTN-NOFDM modulation, an efficient decoder that can recover the transmitted symbols S from the vector R is crucial for such a system.

In the widely used ID algorithm [16], S can be reconstructed by iterating the following equation,

$$\breve{S}_q = R + (e - C)\, \breve{S}_{q-1}, \tag{9}$$

where $\breve{S}_q$ denotes the estimated symbols after q iterations, $\breve{S}_{q-1}$ is the estimated symbols after $q-1$ iterations, e is an $N \times N$ identity matrix, and C is a real-valued $N \times N$ correlation matrix defined as

$$C = F^* F. \tag{10}$$

It should be noted that the initial condition $\breve{S}_0$ is set to R in this algorithm. Then, the soft decision is applied to the estimated symbols after each iteration. The soft mapping strategy of 4-QAM ID is illustrated in Fig. 5(a), where the threshold interval

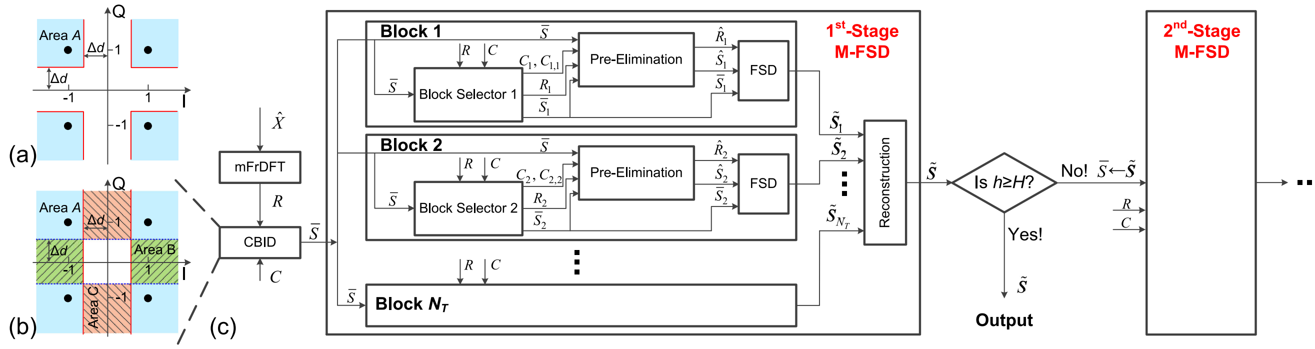

Fig. 5. Mapping strategy of (a) 4-QAM ID, and (b) 4-QAM CBID. (c) Block diagram of the proposed BSSDD.

in each decision is

$$\Delta d = 1 - \frac{q}{Q}, \tag{11}$$

where Q is the total number of iterations. However, in this case, only symbols in area A are made decisions in each iteration, which is not optimized in terms of the utilization of in-phase and quadrature components.

Hence, reference [17] recently proposed an optimized mapping strategy by detecting in-phase and quadrature components separately, as shown in Fig. 5(b). In this algorithm, the symbols in area A, B, or C can all be made decisions accordingly. Besides, this modified decoder named CBID can also be easily applied to the higher order square QAM formats, such as 16-QAM and 64-QAM. Compared to ID based algorithm [25], CBID does not need to design a new mapping strategy for higher-order constellations, leading to the reduced complexity and improved compatibility.

Owing to the advantages discussed above, we employ CBID for pre-decision in our proposed BSSDD, as shown in Fig. 5(c). The accurate estimation from the first-step detection can significantly reduce the computational complexity of the second-step detection that is based on block segmented FSD.

FSD was first proposed in a multiple input multiple output (MIMO) system to significantly reduce the complexity of the original sphere decoding, at the expense of a small loss in performance [26]. In FTN-NOFDM systems, ID-FSD was also investigated to achieve a better ICI-elimination performance than ID [18]. However, such a decoder would greatly limit the number of subcarriers as well as the consequent system flexibility, especially when the adaptive loading is employed [27], [28]. Recently, the multi-FSD based BED was proposed to detect the large-size FTN-NOFDM signal [19]. However, in this case, ID rather than CBID is employed for coarse estimation. Moreover, BED requires the detected FTN-NOFDM signal that is also divided into several blocks by some deleted subcarriers, which changes the signal architecture and reduces the overall SE.

Hence, BSSDD is designed in this work to detect the proposed mFrDFT based FTN-NOFDM signal with improved performance and relatively low complexity. Fig. 5(c) illustrates the principle of the proposed BSSDD. After performing CBID, the constrained estimated symbols $\bar{S}$ are sent to the 1st-stage multi-FSD (M-FSD) module. Such a module is composed of $N_T\,(=N/(2N_B))$ blocks, where N_B denotes the block size, and a factor of 2 is provided by Hermitian symmetry. In each block, the corresponding matrices and symbols are first extracted from the initially obtained C, R and $\bar{S}$ by a block selector as follows:

$$C_{n_T} = \begin{bmatrix} c_{(n_T-1)N_B,0} & \cdots & c_{(n_T-1)N_B,N-1} \\ \vdots & \ddots & \vdots \\ c_{n_T N_B-1,0} & \cdots & c_{n_T N_B-1,N-1} \end{bmatrix}, \tag{12}$$

$$C_{n_T,n_T} = \begin{bmatrix} c_{(n_T-1)N_B,(n_T-1)N_B} & \cdots & c_{(n_T-1)N_B,n_T N_B-1} \\ \vdots & \ddots & \vdots \\ c_{n_T N_B-1,(n_T-1)N_B} & \cdots & c_{n_T N_B-1,n_T N_B-1} \end{bmatrix}, \tag{13}$$

$$R_{n_T} = [r_{(n_T-1)N_B}, \ldots, r_{n_T N_B-1}]^T, \tag{14}$$

$$\bar{S}_{n_T} = [\bar{s}_{(n_T-1)N_B}, \ldots, \bar{s}_{n_T N_B-1}]^T \tag{15}$$

for $n_T = 1, 2, \ldots, N_T$.

Here, C_{n_T} is an $N_B \times N$ submatrix of correlation matrix C; C_{n_T,n_T} is an $N_B \times N_B$ submatrix of correlation matrix C; R_{n_T} is an N_B-dimensional sub-vector of the initially received symbols R in Eq. (8); $\bar{S}_{n_T}$ is an N_B-dimensional sub-vector of the constrained estimated symbols $\bar{S}$ from CBID. Then, in each block, the out-of-block interference can be eliminated from the received symbols by

$$\hat{R}_{n_T} = R_{n_T} - C_{n_T}\bar{S} + C_{n_T,n_T}\bar{S}_{n_T}, \tag{16}$$

In this process, the unconstrained estimated symbols for FSD are also obtained as

$$\hat{S}_{n_T} = \hat{R}_{n_T} + (e_{N_B} - C_{n_T,n_T})\bar{S}_{n_T}, \tag{17}$$

where e_{N_B} is an $N_B \times N_B$ identity matrix. Then, the obtained $\hat{R}_{n_T}$, $\bar{S}_{n_T}$ and $\hat{S}_{n_T}$ in each block are sent to a typical small-dimensional FSD in order to recover the original signal [18], [26]. Such a decision process is implemented by

$$\tilde{S}_{n_T} = \arg \min_{S_{n_T} \in O^V} \left\| \hat{R}_{n_T} - C_{n_T,n_T} S_{n_T} \right\|^2 \le \breve{g}_{n_T}, \tag{18}$$

$$\breve{g}_{n_T} = \left\| \hat{R}_{n_T} - C_{n_T,n_T}\bar{S}_{n_T} \right\|^2, \tag{19}$$

TABLE II
COMPUTATIONAL COMPLEXITY OF DIFFERENT DECODERS

	H-order BSSDD	ID-FSD [18]	CBID [17]
Calculated Branches	$HN_T\left[N_W{}^{W_F}\right]\left[N_P\left(N_B-W_F\right)\right]$	$\left[N_W{}^{W_F N_T}\right]\left[N_P N_T\left(N_B-W_F\right)\right]$	0

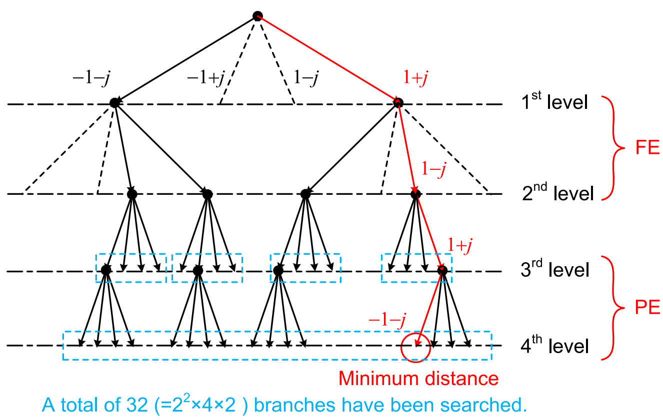

Fig. 6. A hypothetical tree structure for FSD ($N_B = 4$, $W_F = 2$, $N_W = 2$, $N_P = 4$).

where $\|\cdot\|$ denotes the Euclidean norm; $\breve{g}_{n_T}$ denotes the initial radius constraint; O^V is the set of all the possible symbols of V-QAM. For instance, $O^V = \{-1-j, -1+j, 1-j, 1+j\}$ for $V = 4$. Since C_{n_T,n_T} is a real-valued Hermitian positive-definite matrix, using Cholesky decomposition [29], Eq. (18) can be transformed for reducing the computational complexity,

$$L_{n_T}^* L_{n_T} = \text{chol}\left\{C_{n_T,n_T}^* C_{n_T,n_T}\right\}, \tag{20}$$

$$\tilde{S}_{n_T} = \arg \min_{S_{n_T}\in O^V} \left\| L_{n_T}\left(\hat{S}_{n_T} - S_{n_T}\right)\right\|^2 \leq \breve{g}_{n_T}, \tag{21}$$

where L_{n_T} is an $N_B \times N_B$ upper triangular matrix. As shown in Fig. 6, the decision process of FSD can be illustrated by the tree structure, which is divided into two parts. For the first W_F levels, a fixed number of nodes $(=N_W)$ in each level are fully searched. Hence, in such part, a total of $N_W^{W_F}$ branches are searched, which is termed as full expansion (FE). For the remaining levels $(=N_B - W_F)$, with the help of Cholesky decomposition, we only need to calculate the squared Euclidean norm of the current branch, which termed as partial expansion (PE). In PE, N_P nodes in each level are searched. Then, only $N_P(N_B - W_F)$ branches are required to calculate its squared Euclidean norm in the second part.

We can see from Eq. (15)–(17) that the accuracy of the out-of-block interference eliminated symbols $\hat{R}_{n_T}$ and the unconstrained estimated symbols $\hat{S}_{n_T}$ significantly depends on the constrained pre-estimated symbols $\bar{S}$. Therefore, in this work, we further propose the structure of high-order BSSDD. After performing FSD, the recovered symbols are combined with that of other blocks for either output or the cascaded M-FSD, as shown in Fig. 5(c). In the high-order BSSDD, the output symbols $\tilde{S}$ of the h^{th}-stage M-FSD also represent the input symbols $\bar{S}$ of the $(h+1)^{\text{th}}$-stage M-FSD ($h = 1, 2, \ldots, H-1$), which improves the detection performance at the expense of moderate complexity.

The computational complexity of a sphere decoding based decoder is mainly attributed to its calculation of the squared Euclidean norm of each branch. Hence, in Table II, we compare the computational complexity of the proposed BSSDD, the conventional ID-FSD [18] and CBID [17], according to the total number of branches required to be searched in one FTN-NOFDM symbol. For the purpose of a fair comparison, the total number of subcarriers for FE is set to the same $(=N_T W_F)$ for these two decoders. We can see from the table that the computational complexity of ID-FSD grows exponentially as N_T increases. However, in the proposed BSSDD, the number of calculated branches is only directly proportional to N_T. Hence, compared to ID-FSD, BSSDD can significantly reduce the computational complexity, especially when the number of modulated subcarriers is large. On the other hand, owing to its high computational complexity, the number of modulated subcarriers in one FTN-NOFDM symbol is usually not more than 16 if ID-FSD is employed for signal detection [20], [21], which would limit its overall performance. For CBID, although there is no requirement of the calculation of branches, its performance has to be significantly limited. The proposed BSSDD thus becomes an attractive solution that can achieve the compromise between performance and computational complexity. Particularly, when $H = 0$, BSSDD is equivalent to CBID, and when $N_T = 1$, BSSDD is equivalent to multi-stage CBID-FSD, also indicating its great compatibility.

VI. EXPERIMENTAL SETUP

The block diagram of the experimental setup and the DSP is depicted in Fig. 7. In the transmitter (TX)-side DSP, a random bit stream was first mapped into 4-QAM symbols. After performing Hermitian symmetry, 63/128 subcarriers were effectively modulated by the obtained 4-QAM symbols, where only the subcarriers with zero frequency were unfilled. Then, the proposed ImFrDFT was employed to implement a real-valued FTN-NOFDM signal. Before parallel-to-serial conversion, the cyclic prefix (CP) was added to combat the CD, where its length was set to 1/16 of one FTN-NOFDM symbol. After the TX-side DSP, the generated digital signal was converted to an analog signal by using a 24-GSa/s arbitrary waveform generator (AWG) (Tektronix 7122C). Therefore, the data rate of this 4-QAM FTN-NOFDM signal was about 22.24 $(= 2 \times 63/128 \times 16/17 \times 24)$ Gb/s. Then, a narrow-linewidth tunable laser with a central wavelength at 1550.129 nm and a Mach-Zehnder modulator (MZM) working at its linear region were used to convert the

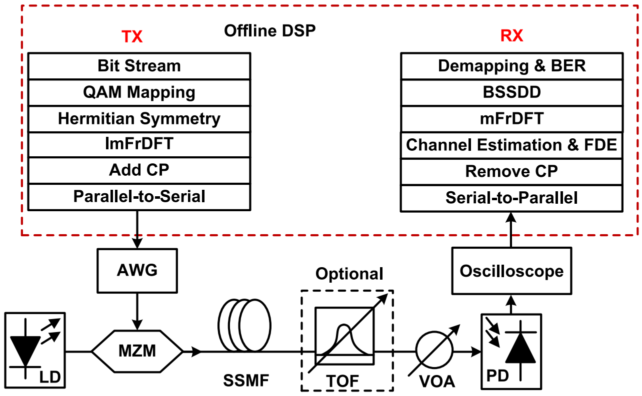

Fig. 7. Experimental setup and DSP for the proposed FTN-NOFDM optical communication system based on IM/DD (AWG: arbitrary waveform generator, LD: laser diode, MZM: Mach-Zehnder modulator, SSMF: standard single mode fiber, TOF: tunable optical filter, VOA: variable optical attenuator, PD: photodiode).

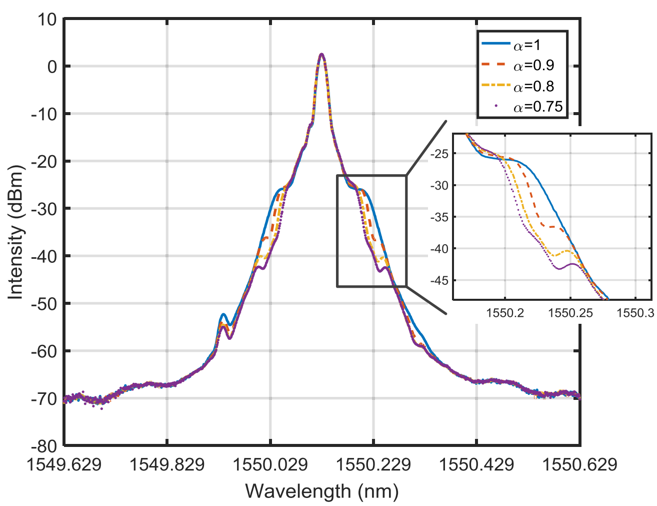

Fig. 8. Measured optical spectra of 24-Gbaud signals with different compression factors at back-to-back (B2B).

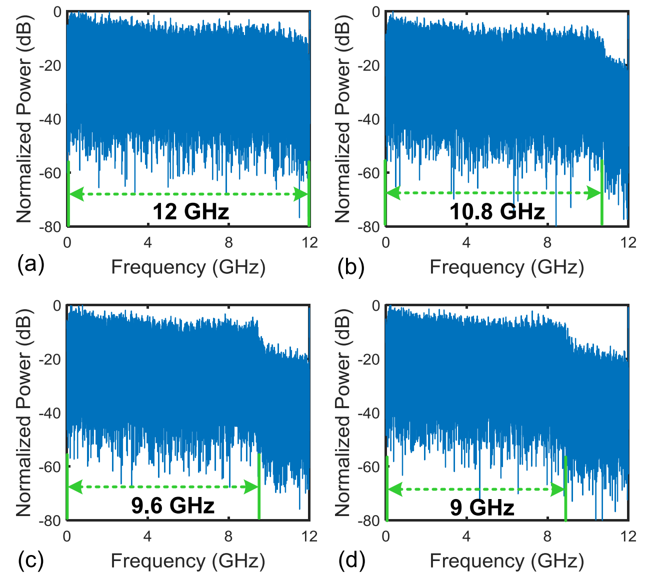

Fig. 9. The electrical spectra of the received FTN-NOFDM signals with a compression factor of (a) 1, (b) 0.9, (c) 0.8, and (d) 0.75, respectively.

obtained electrical signal into the optical domain. Before feeding into a fiber link, we first measured the optical spectra of 24-Gbaud signals with different compression factors. As shown in Fig. 8, we can see that the FTN-NOFDM signal reserves more energy in the lower frequency part as the value of α decreases. Moreover, in the proposed system, no additional guard band between optical carrier and signal is required, which can further improve its tolerance to CD and narrow-band filtering.

After transmission over a piece of 20-km standard single mode fiber (SSMF), a variable optical attenuator (VOA) was applied to control the received optical power (ROP) into the photodiode (PD). Then, the captured optical signal was converted into the electrical domain by a PD (XPDV 2020R). Before performing the receiver (RX)-side DSP, a real-time oscilloscope (Tektronix DSA72004B) at a sampling rate of 50 GSa/s was used to sample the detected FTN-NOFDM signal. The electrical spectra of the received FTN-NOFDM signals with different compression factors are presented in Fig. 9. The obtained samples were then processed by the following steps, including serial-to-parallel conversion, CP removal, channel estimation and the corresponding frequency-domain equalization (FDE), demodulation based on mFrDFT, ICI elimination based on BSSDD, QAM demapping and BER calculation.

V. Results and Discussions

Fig. 10 presents the transmission performance of the proposed 4-QAM FTN-NOFDM IM/DD optical system with different values of α. In consideration of the tradeoff between the computational complexity and the overall performance, the corresponding parameters of BSSDD were set as follows: order of BSSDD $H = 3$, block size $N_B = 16$, block number $N_T = 64/16 = 4$, subcarrier number for FE in each block $W_F = 4$, constellation point number for FE in each subcarrier $N_W = 2$, constellation point number for PE in each subcarrier $N_P = 4$. To verify the feasibility of the proposed decoder, we measured the BER employing BSSDD and CBID [13], respectively. The BER versus ROP in the back-to-back (B2B) system is shown in Fig. 10(a). We can see that the FTN-NOFDM signal with $\alpha = 0.9$ has almost the same performance as the conventional OFDM signal ($\alpha = 1$) in spite of the inherent ICI induced. This can be attributed to its saved bandwidth and consequently higher tolerance to the bandwidth limitation from devices. On the other hand, despite its slight improvement for the FTN-NOFDM signal with $\alpha = 0.9$, the proposed BSSDD can achieve a significant receiver sensitivity improvement compared to CBID when the compression effect is further enhanced. In the case of $\alpha = 0.8$, the required ROP to meet the KP4-forward error correction (FEC) threshold of 2.2 $\times\ 10^{-4}$ is decreased by about 2.5 dB by employing the 3rd-order BSSDD. When 25% bandwidth is saved ($\alpha = 0.75$), compared to CBID, BSSDD can achieve about 1.5-dB receiver sensitivity improvement at the hard-decision (HD) -FEC threshold of 3.8 $\times$

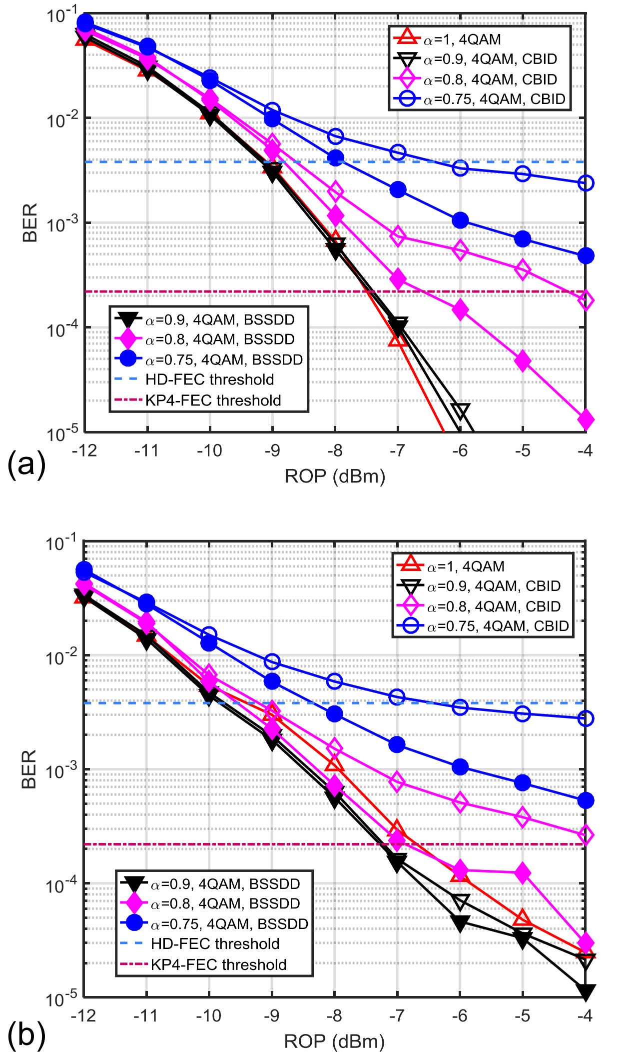

Fig. 10. Measured BER versus ROP (a) at B2B and (b) after 20-km SSMF transmission, for different 4-QAM FTN-NOFDM signals, respectively employing CBID and the 3rd-order BSSDD ($H = 3$, $N = 128$, $N_B = 16$, $N_T = 4$, $W_F = 4$, $N_W = 2$, $N_P = 4$).

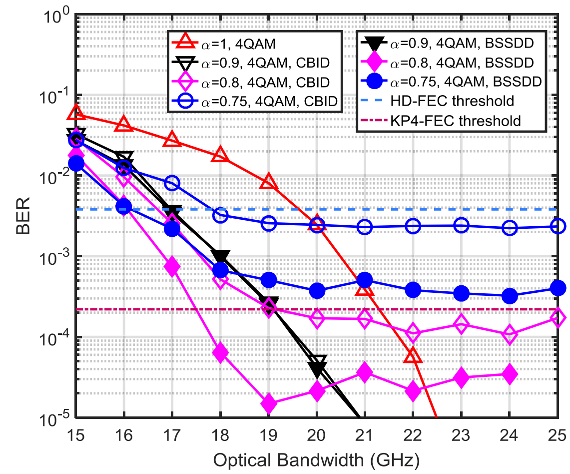

Fig. 11. Measured BER versus optical bandwidth for different 4-QAM FTN-NOFDM signals (B2B, ROP = − 2 dBm).

10^{-3}. Then, we added a piece of 20-km SSMF and measured the corresponding BER under different ROP values, as depicted in Fig. 10(b). Due to bandwidth saving, the FTN-NOFDM signal shows a higher tolerance to the induced CD. We can see from the figure that the proposed scheme with α of 0.9 can even slightly outperform the conventional OFDM signal after 20-km SSMF transmission. On the other hand, when $\alpha = 0.75$, about 2-dB performance improvement is also achieved by using BSSDD in this case.

In this work, we have further investigated the tolerance to system bandwidth limitation for different FTN-NOFDM signals, as shown in Fig. 11. In the B2B system, we used an additional tunable optical filter (TOF) before PD to emulate different system bandwidth values, where ROP was fixed as −2 dBm. We can see from the figure that all these signals with employing FTN-NOFDM outperform the conventional OFDM signal in the bandwidth-limited region. Especially when the 3rd-order BSSDD was also employed, more than 3.5-GHz bandwidth sensitivity improvement can be achieved at both HD-FEC and KP4-FEC thresholds, compared to the conventional OFDM signal. On the other hand, compared to CBID, BSSDD shows about 1.5-GHz improvement at KP4-FEC threshold and 2-GHz improvement at HD-FEC threshold for the cases of $\alpha = 0.8$ and $\alpha = 0.75$, respectively.

From Fig. 10–11, we can see that the optimal compression factor of FTN-NOFDM signals is different for different channel conditions. Therefore, as shown in Fig. 12, we further investigated BER versus α under different optical bandwidth (OBW) limitations and SSMF lengths, via numerical simulations. Herein, optical signal-to-noise ratio (OSNR) was fixed at 20 dB, OBW was emulated by a 4th order Butterworth filter, and the other parameters were set to the same as our experiments. We can see from the figure that the proposed FTN-NOFDM technique with BSSDD achieves improved resilience to the channel impairments, compared to the OFDM signal ($\alpha = 1$). The simulation results also indicate that there is an optimal α for the FTN-NOFDM system, which is dependent on the practical channel condition.

Since FTN-NOFDM can save bandwidth resources, it has great potential to be used in wavelength division multiplexing (WDM) systems. By simulations, we investigated the performance of a 3×24 Gbaud FTN-NOFDM WDM system. Fig. 13 shows BER versus channel spacing for all three channels, where the channel spacing was determined by a Kaiser window. Moreover, the compression factor of FTN-NOFDM signals was set to match with the channel spacing. We can see from the figure that due to its improved resilience to CD, the WDM signals with 21-GHz channel spacing achieve the lowest BER, while saving 12.5% (=3/24) bandwidth. Channel 2 shows slightly poorer performance than the other two channels, which can be attributed to its more severe spectrum overlapping.

As we discussed in Section III, one advantage of the proposed BSSDD is its relatively easy upgrade path to the higher order square QAM formats. Hence, we have also investigated the

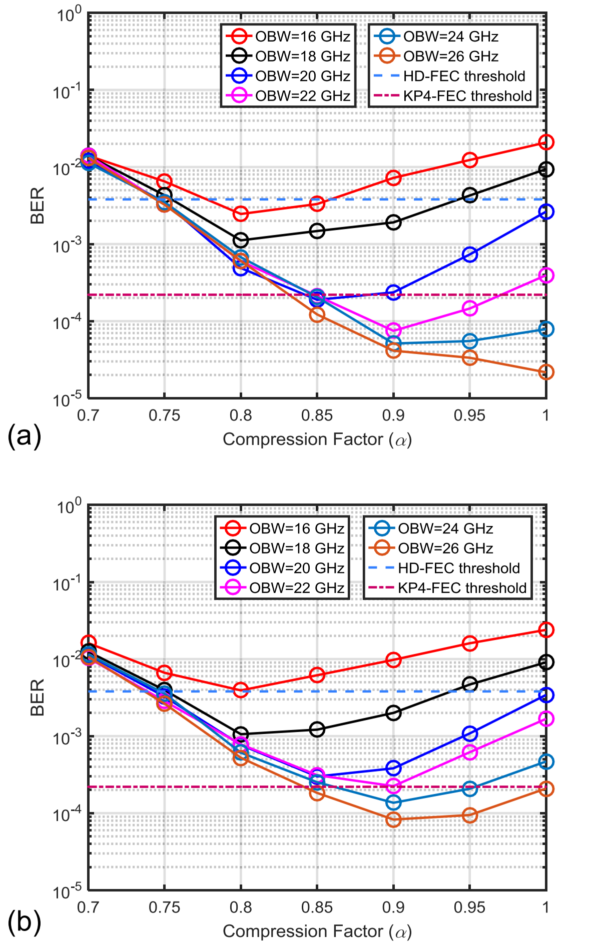

Fig. 12. Under different OBW limitations, BER versus compression factor (a) at B2B and (b) after 20-km SSMF transmission.

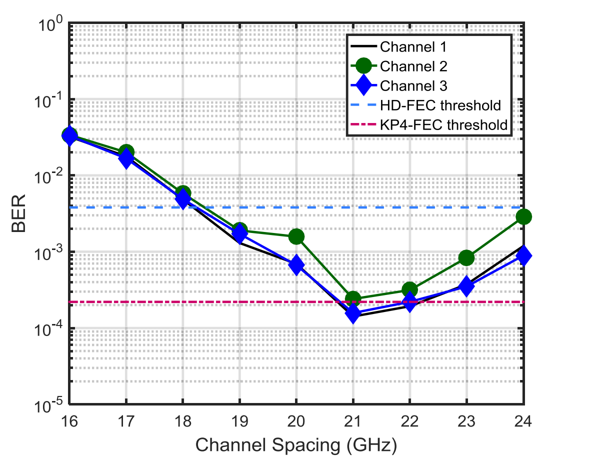

Fig. 13. BER versus channel spacing in a 3 × 24 Gbaud FTN-NOFDM WDM system (20-km SSMF, 20-dB in-band OSNR).

performance of 16-QAM FTN-NOFDM signals using BSSDD. In this case, the AWG sampling rate was set to 12 GSa/s to maintain the data rate as about 22.24 (= 4 × 63/128 × 16/17 × 12) Gb/s, which is the same as the aforementioned 4-QAM FTN-NOFDM signals. As shown in Table II, increasing N_W and W_F would exponentially increase the computational complexity

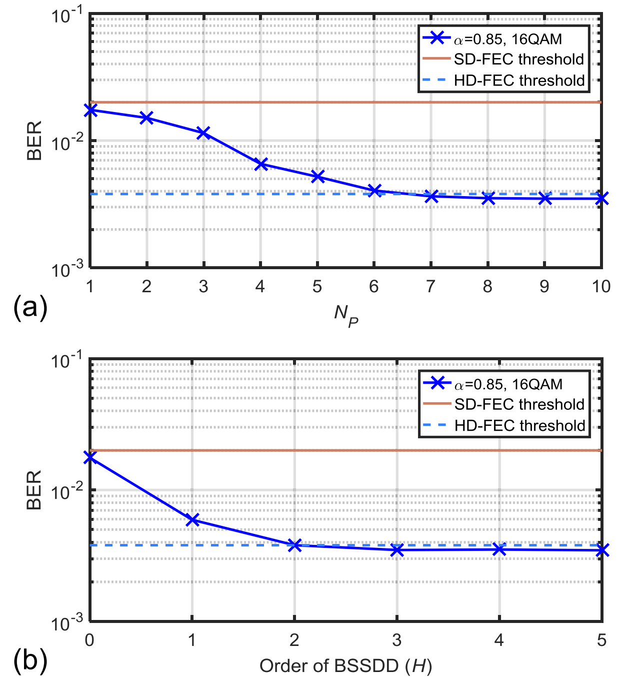

Fig. 14. Dependence of BER on N_P and H for the 16-QAM FTN-NOFDM signal with α of 0.85.

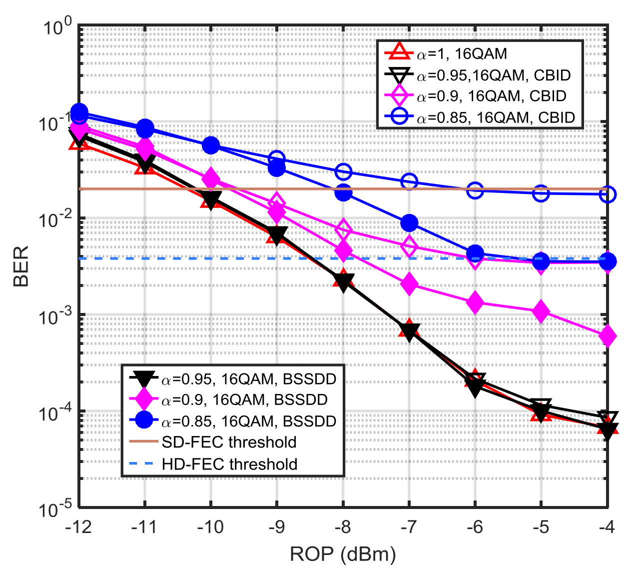

Fig. 15. The performance after 20-km SSMF transmission for different 16-QAM FTN-NOFDM signals, employing CBID and the 3rd-order BSSDD ($H = 3$, $N = 128$, $N_B = 16$, $N_T = 4$, $W_F = 2$, $N_W = 4$, $N_P = 8$), respectively.

of BSSDD. Hence, we optimized the value of N_P and the order of BSSDD: H, as shown in Fig. 14(a) and (b), respectively. We can see from the figure that the optimal values for N_P and H are found to be 8 and 3, respectively. The other parameters were set as follows: $N_B = 16$, $N_T = 64/16 = 4$, $N_W = 4$, $W_F = 2$.

Then, the transmission performance of 22.24-Gb/s 16-QAM FTN-NOFDM signals after 20-km SSMF transmission is depicted in Fig. 15. Despite the severe ICI induced by non-orthogonality, the 16-QAM FTN-NOFDM signal with 15%

bandwidth saving ($\alpha = 0.85$) can still keep its BER below the HD-FEC threshold by employing the proposed BSSDD. Moreover, compared to CBID, BSSDD achieves about 2-dB receiver sensitivity improvement at both HD-FEC threshold and soft-decision (SD) -FEC threshold when α is 0.9 and 0.85, respectively, indicating the enhancement of ICI elimination in an FTN-NOFDM IM/DD optical system.

VI. Summary

In this paper, we have fully investigated our recently proposed mFrDFT based FTN-NOFDM generation method for IM/DD optical communications systems. Without the complicated up-conversion, the bandwidth requirement is further reduced. Moreover, the proposed scheme has no constraint on the compression factor and modulation formats, leading to the improved compatibility and flexibility. For the purpose of efficient symbol detection in a large-size and high-order FTN-NOFDM system, a novel soft-decision decoder, termed as BSSDD, has been further proposed, which can achieve the compromise between performance and computational complexity. We have compared the computational complexity of the proposed BSSDD and the conventional ID-FSD, indicating its significant advantage when the number of subcarriers is large. A 22.24-Gb/s 4-QAM FTN-NOFDM signal with up to 25% bandwidth saving has been experimentally demonstrated over 20-km SSMF while keeping the BER below the HD-FEC threshold. For both 4-QAM and 16-QAM FTN-NOFDM systems, the proposed BSSDD achieves better performance than the conventional CBID. The proposed scheme also shows a higher tolerance to narrow-bandwidth filtering, indicating the great potential of the proposed FTN-NOFDM technique for bandwidth-limited high-speed IM/DD optical systems.

References

[1] E. Ip, A. P. T. Lau, D. J. Barros, and J. M. Kahn, "Coherent detection in optical fiber systems," *Opt. Express*, vol. 16, no. 2, pp. 753–791, Jan. 2008.

[2] D. Qian, N. Cvijetic, J. Hu, and T. Wang, "108 Gb/s OFDMA-PON with polarization multiplexing and direct detection," *J. Lightw. Technol.*, vol. 28, no. 4, pp. 484–493, Feb. 2010.

[3] F. Chang and S. Bhoja, "New paradigm shift to PAM4 signaling at 100/400G for cloud data centers: A performance review," in *Proc. Eur. Conf. Opt. Commun.*, Gothenburg, Sweden, 2017, Paper W.1.A.5.

[4] M. A. Khalighi and M. Uysal, "Survey on free space optical communication: A communication theory perspective," *IEEE Commun. Surv. Tut.*, vol. 16, no. 4, pp. 2231–2258, Fourth quarter 2014.

[5] J. E. Mazo, "Faster-than-Nyquist signaling," *Bell Syst. Tech. J.*, vol. 54, pp. 1451–1462, Oct. 1975.

[6] F. Rusek and J. B. Anderson, "The two dimensional Mazo limit," in *Proc. IEEE Int. Symp. Inf. Theory*, Adelaide, Australia, Sep. 2005, pp. 970–974.

[7] J. B. Anderson, F. Rusek, and V. Owall, "Faster-than-Nyquist signaling," *Proc. IEEE*, vol. 101, no. 8, pp. 1817–1830, Aug. 2013.

[8] A. D. Liveris and C. N. Georghiades, "Exploiting faster-than-nyquist signaling," *IEEE Trans. Commun.*, vol. 51, no. 9, pp. 1502–1511, Sep. 2003.

[9] M. Rodrigues and I. Darwazeh, "A spectrally efficient frequency division multiplexing based communications system," in *Proc. 8th Int. OFDM Workshop*, Hamburg, Germany, 2003, pp. 48–49.

[10] J. Zhou, Y. Qiao, Z. Yang, and E. Sun, "Faster-than-nyquist non-orthogonal frequency-division multiplexing based on fractional hartley transform," *Opt. Lett.*, vol. 41, no. 19, pp. 4488–4491, Oct. 2016.

[11] J. Zhou *et al.*, "Capacity limit for faster-than-Nyquist non-orthogonal frequency-division multiplexing signaling," *Sci. Rep.*, vol. 7, Jun. 2017, Art. no. 3380.

[12] J. Zhao and L. K. Chen, "Adaptively loaded IM/DD optical OFDM based on set-partitioned QAM formats," *Opt. Express*, vol. 25, no. 8, pp. 9368–9377, Apr. 2017.

[13] J. Zhao, "DFT-based offset-QAM OFDM for optical communications," *Opt. Express*, vol. 22, no. 1, pp. 1114–1126, Jan. 2014.

[14] Z. Hu and C. K. Chan, "A modified fractional DFT based FTN-NOFDM technique for IM/DD optical systems," in *Proc. Opto-Electron. Commun. Conf.*, Jeju, South Korea, Jul. 2018, Paper 3B1-4.

[15] Z. Hu, S. Gao, Y. Shao, L. K. Chen, and C. K. Chan, "A robust channel processor for faster-than-nyquist non-orthogonal FDM visible light communication systems," in *Proc. Eur. Conf. Exhib. Opt. Commun.*, Rome, Italy, Sep. 2018, Paper Th2. 18.

[16] S. Heydari, M. Ferdosizadeh, and F. Marvasti, "Iterative detection with soft decision in spectrally efficient FDM systems," Apr. 2013, *arXiv:1304.4003v1*.

[17] J. Huang, Q. Sui, Z. Li, and F. Ji, "Experimental demonstration of 16-QAM DD-SEFDM with cascaded BPSK iterative detection," *IEEE Photon. J.*, vol. 8, no. 3, pp. 1–9, Jun. 2016.

[18] T. Xu, R. Grammenos, F. Marvasti, and I. Darwazeh, "An improved fixed sphere decoder employing soft decision for the detection of non-orthogonal signals," *IEEE Commun. Lett.*, vol. 17, no. 10, pp. 1964–1967, Oct. 2013.

[19] T. Xu and I. Darwazeh, "Multi-band reduced complexity spectrally efficient FDM systems," in *Proc. 9th IEEE/IET Int. Symp. Commun. Syst., Netw. Digit. Sign*, Manchester, U.K., Jul. 2014, pp. 904–909.

[20] I. Darwazeh, T. Xu, T. Gui, Y. Bao, and Z. Li, "Optical SEFDM system; bandwidth saving using non-orthogonal sub-carriers," *IEEE Photon. Technol. Lett.*, vol. 26, no. 4, pp. 352–355, Feb. 2014.

[21] Y. Wang *et al.*, "SEFDM based spectrum compressed VLC system using RLS time-domain channel estimation and ID-FSD hybrid decoder," in *Proc. 42nd Eur. Conf. Exhib. Opt. Commun.*, Düsseldorf, Germany, Sep. 2016, pp. 827–829.

[22] T. Xu, S. Mikroulis, J. E. Mitchell, and I. Darwazeh, "Bandwidth compressed waveform for 60-GHz millimeter-wave radio over fiber experiment," *J. Lightw. Technol.*, vol. 34, no. 14, pp. 3458–3465, Jul. 2016.

[23] P. Whatmough, M. Perrett, S. Isam, and I. Darwazeh, "VLSI architecture for a reconfigurable spectrally efficient FDM baseband transmitter," *IEEE Trans. Circuits Syst. I, Reg. Papers*, vol. 59, no. 5, pp. 1107–1118, May 2012.

[24] C. Guo *et al.*, "98.7-Gb/s Optical SE-DMT transmission using an enhanced decision-directed algorithm with preconditions," in *Proc. Asia Commun. Photon. Conf.*, Guangzhou, China, 2017, Paper S4B-2.

[25] T. Xu and I. Darwazeh, "M-QAM signal detection for a non-orthogonal system using an improved fixed sphere decoder," in *Proc. 9th IEEE/IET Int. Symp. Commun. Syst., Netw. Digit. Sign*, Manchester, U.K., Jul. 2014, pp. 623–627.

[26] L. G. Barbero and J. S. Thompson, "A fixed-complexity MIMO detector based on the complex sphere decoder," in *Proc. IEEE Int. Workshop Signal Process. Adv. Wireless Commun.*, Jul. 2006, pp. 1–5.

[27] P. S. Chow, J. M. Cioffi, and J. A. C. Bingham, "A practical discrete multitone transceiver loading algorithm for data transmission over spectrally shaped channels," *IEEE Trans. Commun.*, vol. 43, no. 2/4, pp. 773–775, Feb./Apr. 1995.

[28] S. C. J. Lee, S. Randel, F. Breyer, and A. M. J. Koonen, "PAM-DMT for intensity-modulated and direct-detection optical communication systems," *IEEE Photon. Technol. Lett.*, vol. 21, no. 23, pp. 1749–1751, Dec. 2009.

[29] R. A. Horn and C. R. Johnson, *Matrix Analysis*. Cambridge, U.K: Cambridge Univ. Press, 1985.